

Article

Effects of Zr Additive on Microstructure, Mechanical Properties, and Fractography of Al-Si Alloy

Hui Qian, Degui Zhu *, Chunfeng Hu and Xiaosong Jiang

Key Laboratory of Advanced Technologies of Materials, Ministry of Education, School of Materials Science and Engineering, Southwest Jiaotong University, Chengdu 610031, China; qianhui@my.swjtu.edu.cn (H.Q.); chfhu@live.cn (C.H.); xsjiang@home.swjtu.edu.cn (X.J.)

* Correspondence: dgzhu@home.swjtu.edu.cn; Tel./Fax: +86-28-8760-0779

Received: 8 January 2018; Accepted: 6 February 2018; Published: 10 February 2018

Abstract: The effects of Zr additive on the microstructure, mechanical properties, and fracture behavior of Al-Si alloy were systematically investigated. The additive of Zr obviously reduced the size of Si particles and changed its morphology. Grain size refinement was promoted by the reaction between Al and Zr forming Al_3Zr and ZrSi_2 compounds. Compared to a Zr-free alloy, the additive enhanced the tensile strength, compressive strength, shear strength, and hardness. The optimized Zr content was 2.4 wt % corresponding to a tensile strength of 231.1 MPa, compressive strength of 343.1 MPa, shear strength of 174.9 MPa, and hardness of 85.5 HV, greater than those of the Zr-free alloy. This illustrates that fine-grain strengthening and the existence of a second phase can improve the mechanical properties of Al-Si alloy. The fracture surface of Al-Si alloy without Zr additive showed a brittle fracture mode and there were no pits on the fractured surface. In the presence of Zr additive, a typical plastic deformation with a large amount of pits was evidenced.

Keywords: Al-Si alloy; hot isostatic pressing (HIP); microstructure; mechanical properties; fracture mechanism

1. Introduction

There is an increasing need of outperforming materials having properties matching societal needs. Among advanced engineering materials for aerospace and automotive applications, Al-based metal matrix composites (MMC) stand out for their excellent mechanical properties, such as low density, high plasticity and strength, and good fatigue and wear resistance [1–5]. Up to now, aluminum–silicon (Al-Si) alloys have been extensively used because of their excellent castability, low coefficient of thermal expansion, good corrosion resistance, and high strength-to-weight ratio [6–8]. Al-based metal matrix composites finds application in many industries, including automotive, military, aerospace, and electronics [9,10]. The limitation of aluminum is still with regard to its low mechanical properties. In previous works [1–24], it was found that the plasticity and wear resistance of Al-Si alloy are reduced because of the presence of undesired thick and irregular silicon precipitates, also causing the poor machinability. There are two different ways to enhance the mechanical properties: one is to act on the processing, the other one is by modifying the chemical composition.

The composition modification has been considered effective to design the morphology and size of silicon particles. Therefore, many chemical elements have been considered for this purpose, these include earth-abundant elements (TiC, TiB_2 , Sr, and Na), and rare earths (Er, Sb, Ce, La, Yb, Eu, and Sc [11–14]. Prukkanon et al. [15] investigated the effect of Sc on the modification of Al-6Si-0.25Mg alloy. Experiments show that the eutectic composition of Al-6Si-0.25Mg can be modified with the addition of Sc as low as 0.2 wt %. Pandee et al. [16] investigated the effect of Er on the micro-structural evolution and mechanical properties of the Al-7Si-0.3Mg alloy, they reported that Er refined the primary Al grain size and eutectic Si particles. With an addition as low as 0.2 wt % Zr, the grain size of

the as-cast alloy was refined, and the solid solution forms a secondary Al_3Zr phase, which enhanced the mechanical strength [17]. The hardness of the A319 aluminum cast alloy in both as-solutionized and age-hardened conditions is improved with small additions of Zr [18]. The effects of the Gd and Zr additions of A356 cast alloys have been systematically investigated with respect to grain size refinement and eutectic Si modification [19], and both Gd and Zr promoted grain refinement of A356 alloy. A fine grain changes the micro-structure of the material, which leads to the change of the mechanical properties. Therefore, it is very meaningful to understand the additive of an alterant on the micro-structure and mechanical properties of Al-Si alloy.

Powder metallurgy (PM) is a well-established method for the fabrication of MMC [20,21]. The pressure-assisted PM method include hot pressing (HP) and hot isostatic pressing (HIP). Most of the literature is focused on HP and only few reports are on use of HIP. In this work, the effect of Zr additive on the micro-structure and mechanical properties of Al-Si alloy prepared using HIP was systematically investigated. The reinforcement mechanisms were also discussed.

2. Experimental Procedure

The quality percentage of different contents in Al-Si alloys were shown in Table 1. The Al-Si alloys with different Zr contents of 0 wt %, 1.0 wt %, 1.5 wt %, and 2.4 wt % were named as Alloy 1, Alloy 2, Alloy 3, and Alloy 4, respectively. Firstly, 128.2 g aluminum powder (50 μm , 99.9%), 13.6 g silica powder (60 nm, 99.9%), and Zr (50 μm , 99.9%) with different quality (0 g in Alloy 1, 1.4 g in Alloy 2, 2.1 g in Alloy 3, and 3.5 g in Alloy 4) were weighed and mixed for one hour using a ball milling machine at room temperature. After freeze drying and sieving, the mixture was loaded in a rubber bag and cold isostatically-pressed under a pressure of 100 MPa. Dense alloy was consolidated by HIP (QIH-15, ABB, Zurich Switzerland) at 800 °C for 30 min under 70 MPa. Specimens were cut using electrical discharge machining. After polishing and ultrasonic cleaning using water and ethanol, the surface of samples was observed using an optical microscope (OM) (Zeiss MFA 2, MF, Jena, Germany).

Table 1. The quality percentage of different contents in experimental alloys.

Alloy	wt % (Al)	wt % (SiO_2)	wt % (Zr)
Alloy 1	90.4	9.6	0
Alloy 2	89.5	9.5	1.0
Alloy 3	89.1	9.4	1.5
Alloy 4	88.2	9.4	2.4

The density of the consolidated samples was evaluated by the Archimedes' principle. The Vickers hardness of Al-Si alloy was measured using a hardness tester (HX-1000TM, Taiming, Shanghai, China) with the load of 100 gf. The tensile, compressive, and shear tests were carried out by using an Instron 4204 universal testing machine (Mini MFA 2, MF, Jena, Germany) at a crossing speed of 1 mm/min. The fracture surface of tensile samples was observed and analyzed using a scanning electron microscope (SEM) (FEI, Hillaboro, OR, USA) equipped with an energy dispersive spectrometer (EDS) (Octance Super, EDAX, Mahwah, NJ, USA). Phase analysis was performed using X-Pert PRO-MPD (PANalytical B.V., Almelo, The Netherlands) with Cu $K\alpha$ radiation.

3. Results and Discussion

3.1. Micro-Structure Characterization

Figure 1 shows the optical microscope images of Al-Si alloys with different Zr amounts. The black arrows points to the silicon particles having different morphology and dimension and, in the unmodified Al-Si alloy, the size of silicon particles (gray area) is very large and have the phenomenon of reunion, as shown in Figure 1a. In contrast, when Zr was added to the Al-Si alloys, the silicon particles

become progressively smaller, as shown in Figure 1b–d. When the Zr additive is 1.0 wt %, the size of dispersive silicon particles was reduced and it distributed uniformly within the matrix, as shown in Figure 1b. When the Zr content is 1.5 wt %, the size of the dispersive silicon particles was reduced compared to the unmodified Al-Si alloys and was not uniform, as shown in Figure 1c. When the Zr content was 2.4 wt %, the size of the dispersive silicon particles was reduced significantly compared to the alloys with other content of Zr and distributed uniformly in the basic material, as shown in Figure 1d. There are no holes in the optical microscope images, as shown in Figure 1, and Table 2 shows the theoretical density and the actual density of four different kinds of Al-Si alloy. The actual density is almost the same with the actual density and that means the Al-Si alloys are compact.

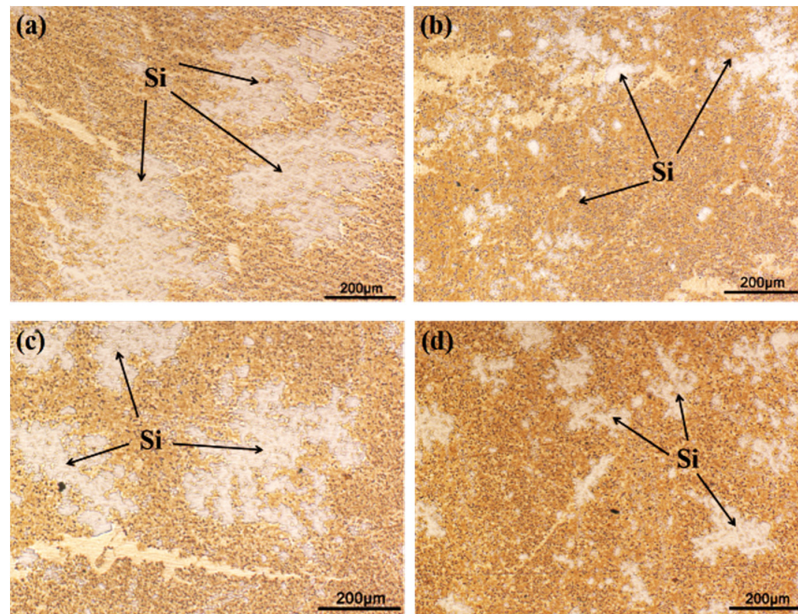


Figure 1. Metallography images of Al-Si alloys with different contents of Zr: (a) unmodified, Alloy 1; (b) 1.0 wt % Zr, Alloy 2; (c) 1.5 wt % Zr, Alloy 3; and (d) 2.4 wt % Zr, Alloy 4.

Table 2. The quality ratio of alloys elements and the quality percentage of Zr.

Alloy	Theoretical Density (g/cm ³)	Actual Density (g/cm ³)
Alloy 1	2.78	2.78 ± 0.02
Alloy 2	2.80	2.82 ± 0.02
Alloy 3	2.80	2.82 ± 0.02
Alloy 4	2.81	2.81 ± 0.02

According to the theory [22], when adding an element to an alloy which has low diffusivity and solubility could relate to grain coarsening. Zr has the lowest diffusion coefficient in aluminum among the transition metals [22], and aluminum base alloys result in the formation of an Al₃Zr phase with the addition of Zr. The XRD result shown in Figure 2d confirmed the formation of Al₃Zr. In binary Al-Zr alloys, Al₃Zr can form either as a semi-coherent tetragonal equilibrium phase or as coherent cubic form. Both forms are expected to form low-energy interfaces with the Al matrix [23]. Due to the low solubility and diffusivity of Zr in the Al matrix, these coherent particles are stable, resulting in Si particle refinement [18].

Figure 3 shows the SEM of Al-Si alloys with different contents of Zr. The size of silicon particles in light gray area is large and evidences the phenomenon of reunion for the unmodified Al-Si alloy, as shown in Figure 3a. In contrast, when Al-Si alloys were modified with the addition of Zr, the size of the silicon particles became smaller, as shown in Figure 3b–d. When the Zr additive was 1.0 wt %, the size of the silicon particles was reduced and it distributed uniformly within the matrix, as shown in Figure 3b. When the Zr content is 1.5 wt %, the size of the dispersive silicon particles was reduced compared to the unmodified Al-Si alloys and was not uniform, as shown in Figure 3c. When the Zr content was 2.4 wt %, the size of the dispersive silicon particles was reduced significantly compared to the alloys with other content of Zr and distributed uniformly in the basic material, as shown in Figure 3d.

there are many second phases, as shown in Figure 3b. When the Zr content was 1.5 wt %, more second phases are evidenced in Figure 3c. When the Zr content is 2.4 wt %, there are many small shiny second phases, more than the other samples (Alloy 1–3), as shown in Figure 3d. According to the binary Al-Zr diagram, dispersoid precipitation is possible when the Zr concentration is greater than 0.08% at a temperature of 500 °C [18]. Here, the dispersoid precipitation is also expected to occur at 800 °C using HIP. A peritectic reaction provides heterogeneous nuclei for α -Al nucleation due to the Al_3Zr particles' formation, leading to the obvious grain refinement [24]. The micro-structure of the Al-based metal matrix composites is not changed with the addition of Zr in the as-cast condition, and the only significant change is the dendrite arm spacing (DAS) which is caused by the Zr [18]. This has also been reported by Prangnell et al. [23], who studied the dispersoid precipitation in Zr-containing Al-based metal matrix composites.

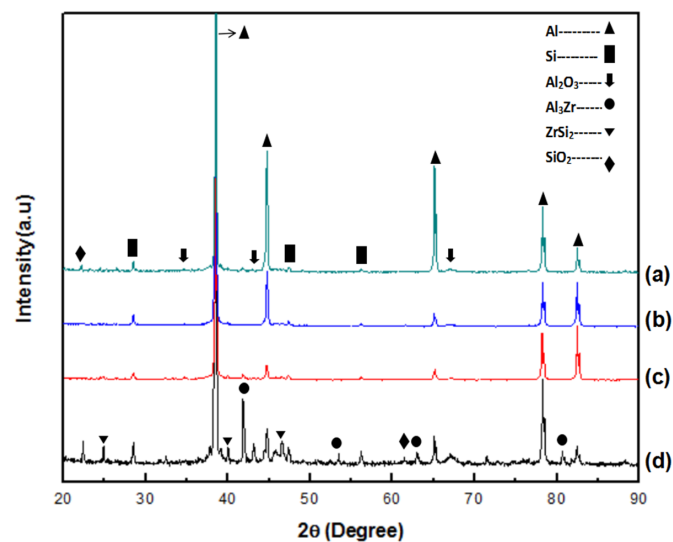


Figure 2. X-ray diffraction (XRD) patterns of Al-Si alloys with different contents of Zr: (a) unmodified, Alloy 1; (b) 1.0 wt % Zr, Alloy 2; (c) 1.5 wt % Zr, Alloy 3; and (d) 2.4 wt % Zr, Alloy 4.

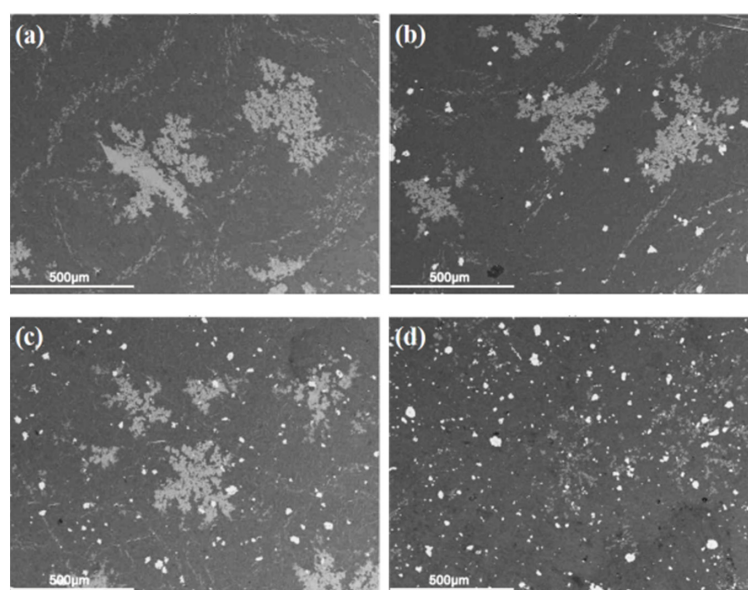


Figure 3. SEM of Al-Si alloys with different Zr content: (a) unmodified, Alloy 1; (b) 1.0 wt % Zr, Alloy 2; (c) 1.5 wt % Zr, Alloy 3; and (d) 2.4 wt % Zr, Alloy 4.

Figure 4 shows the elemental mapping results. The main elements of the second phase are Al, Si, and Zr. Figure 5 shows the EDS results of the second phase, and the fractions of the Al, Si, and Zr were about 67.47%, 11.9%, and 20.63%. Combined with the XRD result, as shown in Figure 2d, the second phase are Al_3Zr and ZrSi_2 —the oxygen from the starting SiO_2 formed Al_2O_3 . Some of the Zr is distributed around the Si, which is related with Si and Al hindering the Si particle growth.

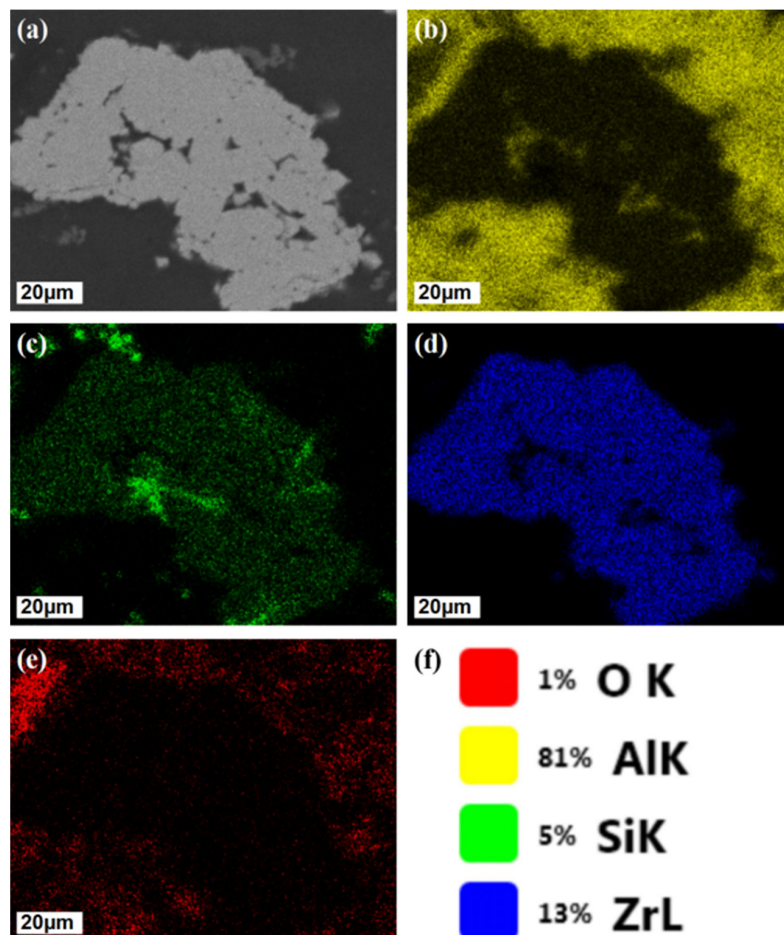


Figure 4. Elemental mapping of sample with the adding of 2.4 wt % Zr in Al-Si alloy: (a) SEM; (b) Al element; (c) Si element; (d) Zr element; (e) O element; and (f) element ratios.

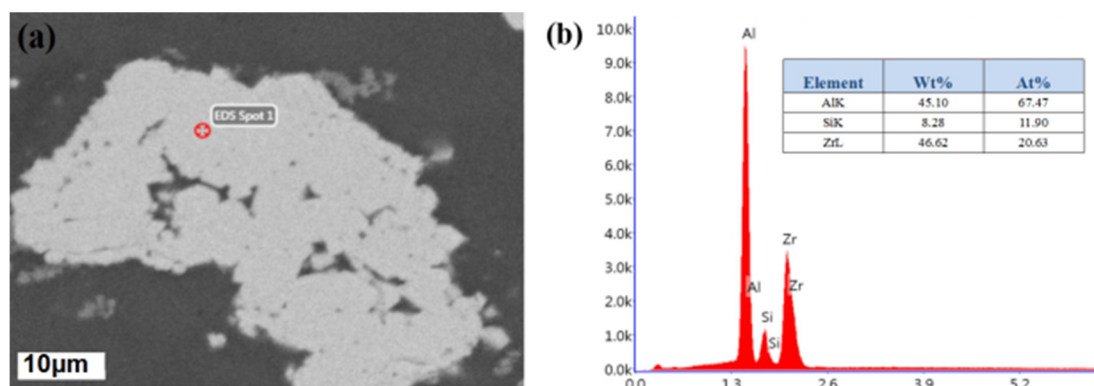


Figure 5. SEM micro-structure and EDS (energy dispersive spectrometer) analysis of the Al-Si alloys with 2.4 wt % Zr: (a) morphology; and (b) EDS of the intermetallic compound containing Al, Si, and Zr.

Figure 6 includes the TEM (transmission electron microscope) (Jeol Inspect F50, Jeol, Tokyo, Japan) images of Al-Si alloys with 2.4 wt % contents of Zr. It could be observed in any areas because the microstructure of Al-Si alloy is uniform. The selected area electron diffraction (SAED) (FEI, Hillaboro, OR, USA) pattern recorded the zone axis of $[02\bar{2}]$ Al and is presented in Figure 7a and the area of the SAED results are shown in Figure 6c. The zone axis of $[\bar{2}20]$ Si is presented in Figure 7b and the area of the SAED results are shown in Figure 6a,b. The zone axis of $[\bar{4}48]$ Al_2O_3 is presented in Figure 7c and the area of the SAED results are shown in Figure 6c. The zone axis of $[6\bar{4}6]$ ZrSi_2 is presented in Figure 7d and the area of the SAED results are shown in Figure 6d. The results in Figures 6 and 7 suggests that the in situ reactions reached competition. Based on the literature [18], the grain of the Al-based metal matrix composites could be refined after adding Zr, leading to the fine-grain strengthening effect. The fine precipitates generated by the reaction with Al-Zr-Si (Al_3Zr and ZrSi_2) induced improvement in mechanical properties described in the section below.

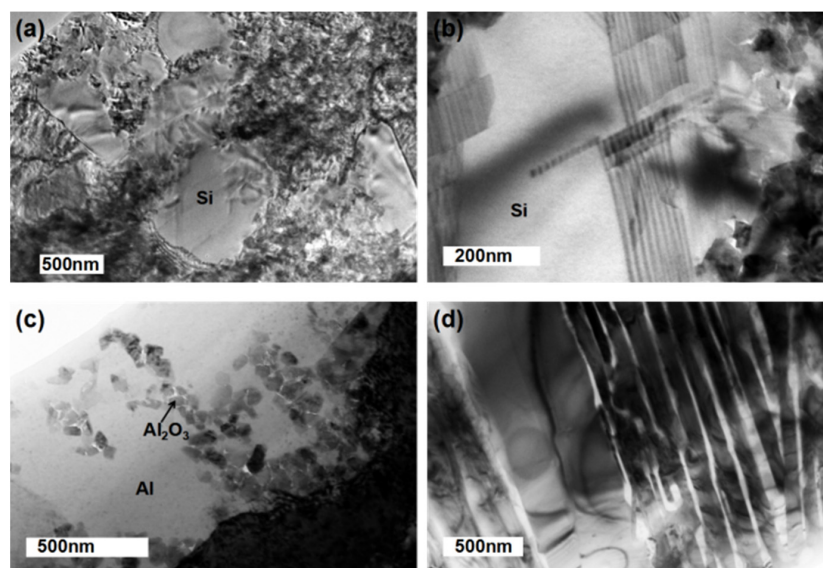


Figure 6. TEM images of Al-Si alloys with 2.4 wt % Zr. (a) Si ; (b) Si after amplification; (c) Aluminium Matrix; (d) the second phase.

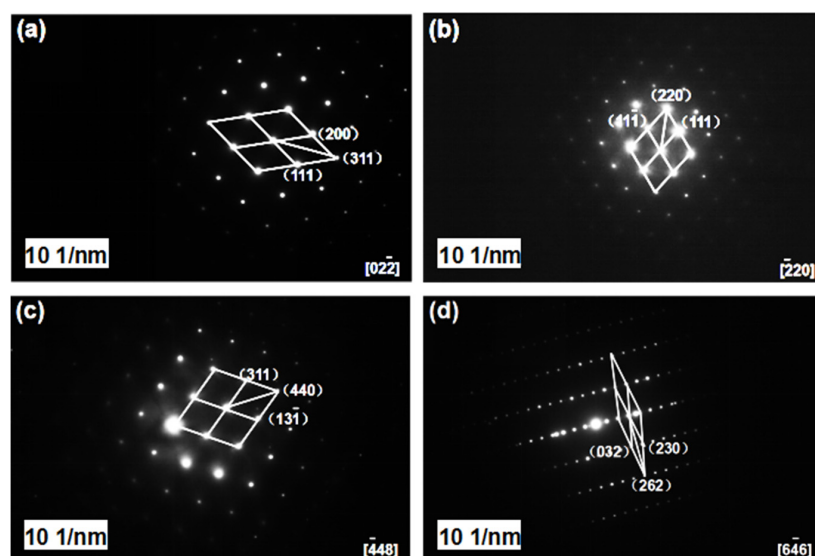


Figure 7. The SAED (selected area electron diffraction) pattern of sample with the adding of 2.4 wt % Zr in Al-Si alloy: (a) Al; (b) Si; (c) Al_2O_3 ; and (d) ZrSi_2 .

3.2. Mechanical Properties

Table 3 lists the tensile strength, yield strength, elongation, compressive strength, shear strength, and hardness of Al-Si alloys with the different Zr contents. The mechanical properties of Al-Si alloys were improved obviously after adding Zr element compared to the unmodified alloys. It is reported that the hardness of the Al-based metal matrix composites is enhanced with small additions of Zr in both as-solutionized and age-hardened conditions [18]. The rather slow kinetics of the dispersoid precipitation requires such a long time to form the precipitation of the Al₃Zr phase during the solutionizing treatment. The same results were confirmed for Al-Si alloy prepared with HIP. The hardness of Al-Si alloys with the additive of 1.0 wt % Zr, 1.5 wt % Zr, and 2.4 wt % Zr was increased up to 82.5 HV, 79.3 HV, and 85.5 HV, respectively, in comparison with the unmodified alloys with the hardness of 65.2 HV. This corresponded to percentage improvements of 6.2, 2.0, and 10.0%. It has been reported that, when adding Zr to A356 + 0.4Gd [22], the mechanical properties (the ultimate tensile strength (UTS) and the yield strengths (YS), along with elongation) were improved with the addition of Zr because of the grain refinement and eutectic Si modification.

The tensile strength, yield strength, elongation, the compressive strength, and the shear strength of Al-Si alloys with the additive of Zr additive were improved. The tensile strength, yield strength, elongation, the compressive strength, and the shear strength of Al-Si alloy with 2.4 wt % Zr was enhanced most significantly, improved to 231.1 MPa, 114.6 MPa, 7.4%, 343.1 MPa, and 174.9 MPa. This illustrates that fine-grain strengthening and the existence of a second phase can improve the mechanical properties of the Al-Si alloy. According to the Hall-Petch equation, the relationship between the grain size and strength follows:

$$\sigma_s = \sigma_i + Kd^{-1/2}$$

where σ_s is the material strength, σ_i and K are two constants which is related to the material, and d is the grain size. Fine-grain strengthening can improve the plasticity, and also enhance toughness. According to the Orowan's theory, dislocation would bypass the intermetallic second phase without leaving the dislocation loop. The second phase (Al₃Zr and ZrSi₂) hinders the movement of a dislocation, which increases the stress of the crystal slip and the density of the dislocations, leading to enhanced mechanical properties. When a second phase is finely distributed within the matrix it will produce a significant reinforcement. The main reason of the second phase strengthening is the interaction between the dislocation, which hinders the motion of the dislocation and improves the mechanical properties of the alloy. Combined with the XRD result, as shown in Figure 2d, the compositions of the second phase are Al₃Zr and ZrSi₂.

Owing to the refining effect and the dispersion strengthening, the mechanical properties of Al-Si alloys were improved markedly with the addition of Zr. The reinforcement was associated with the formation of Al₃Zr and ZrSi₂. With increasing Zr content, the Si eutectic was modified little after adding Zr because the formation was Zr-rich [18].

Table 3. The mechanical properties of Al-Si alloys with different Zr content.

Alloy	Tensile Strength (MPa)	Yield Strength (MPa)	Elongation (%)	Compressive Strength (MPa)	Shear Strength (MPa)	Hardness (HV)
Alloy 1	211.2 ± 7.2	89.1 ± 7.9	5.7 ± 0.3	299.6 ± 22.6	151.6 ± 3.7	65.2 ± 7.2
Alloy 2	224.2 ± 10.2	99.1 ± 8.5	6.5 ± 0.3	337.8 ± 28.8	171.3 ± 4.5	82.5 ± 10.2
Alloy 3	221.6 ± 9.0	98.4 ± 6.7	6.7 ± 0.2	330.6 ± 32.3	174.7 ± 7.7	79.3 ± 9.4
Alloy 4	231.1 ± 15.4	114.6 ± 9.7	7.4 ± 0.7	343.1 ± 24.4	174.9 ± 5.5	85.5 ± 11.6

3.3. Fractography

Figure 8 summarizes the SEM fractographs of Al-Si alloys with different Zr content. It is seen that the fracture surface of the Al-Si unmodified alloy shows a clear brittle fracture mode. Few dimples appeared on the fracture surface of Al-Si unmodified alloy, and a quasi-cleavage feature can be observed in Figure 8a. The number of the dimples increases significantly when adding Zr, as shown in Figure 8b–d. The obvious grain refinement and eutectic Si modification led to improved mechanical properties [18]. The ductile fracture confirmed a peeling process and energy was consumed. The ductile fracture surface shows the parallel or 45° angle with respect to the maximum shear stress. The fracture surface of the Al-Si modified alloy with the addition of 1.5 wt % Zr displayed a mixed quasi-cleavage and dimple morphology. Brittle fracture, which presents as flakes under the dimples, is shown in Figure 8c. The fracture surface of the Al-Si modified alloy with the addition of 1.0 wt % Zr shows the smaller and greater number of uniformly distributed dimples. The fracture surface evidences a ductile mode (Figure 8b).

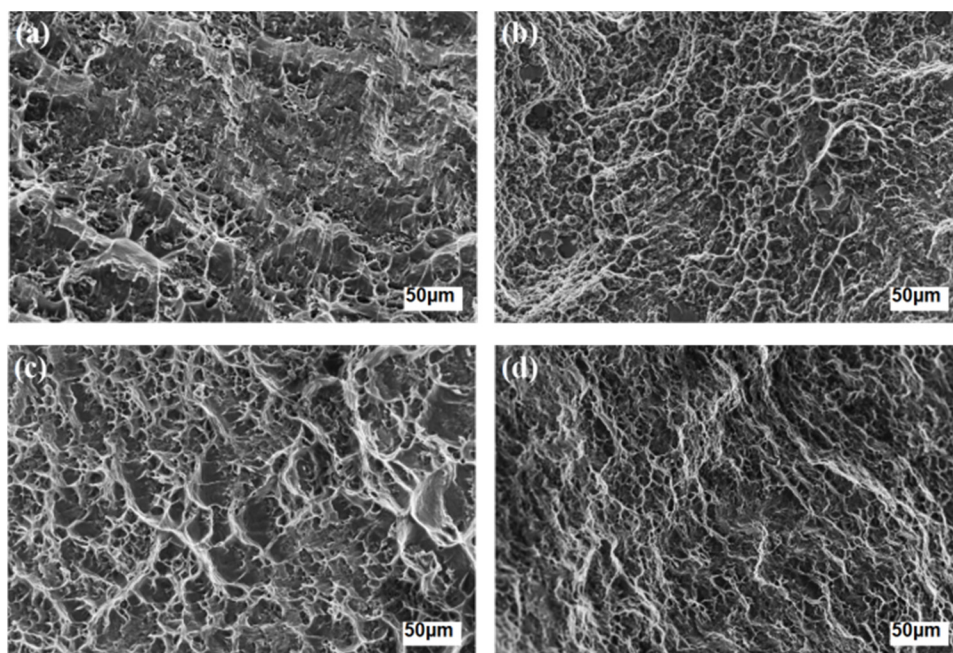


Figure 8. Scanning electron microscope (SEM) graphs of tensile fracture surface of Al-Si alloys with different content of Zr: (a) unmodified, Alloy 1; (b) 1.0 wt % Zr, Alloy 2; (c) 1.5 wt % Zr, Alloy 3; and (d) 2.4 wt % Zr, Alloy 4.

Figure 9 shows the SEM micro-structure and EDS analysis of the fracture surface of Al-Si alloy with the addition of 2.4 wt % Zr. In agreement with the results in Figure 3 and the EDS results shown in Figure 9b, the second phase composition was 68.88% Al, 11.69% Si, and 19.44% Zr. As shown in Figure 9a, the deformation time is not same of the substrate and the second phase of the different plasticity. Based on the theory of the dislocation, the critical cutting stress of the slip system is different between different grains under the action of the external force because the orientation is different between different grains in poly crystal. The Al grain deforms earlier than the second phase because of the favorable orientation. The plastic deformation of Al will be constrained by the rigid second phase, leading to an increased deformation resistance and tensile properties.

The tensile fracture surface of Al evidences a plastic fracture characteristic like potholes because of its plasticity. The tensile fracture surface of Si presents a brittle fracture characteristic like crisp flakes typical of a brittle material. There are vast regions that present the flake fracture in unmodified Al-Si

alloy because of the Si particles. After adding Zr to the Al-Si alloy, the dimension of the Si particles was reduced distinctly, leading to the plastic fracture surface like potholes.

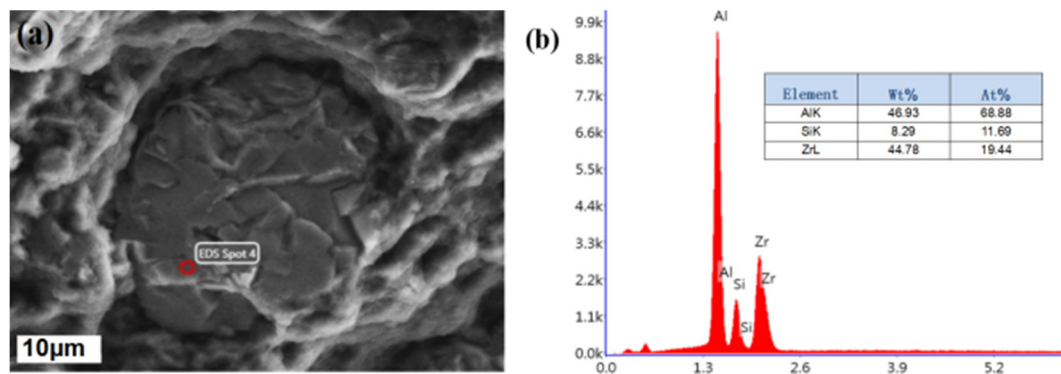


Figure 9. Scanning electron microscope (SEM) graphs of tensile fracture surface of Al-Si alloys: (a) morphology; and (b) EDS of the intermetallic compound containing Al, Si, and Zr.

4. Conclusions

The effects of Zr additive on the micro-structure and mechanical properties of Al-Si alloys were investigated. The results can be summarized as follows:

- (1) The size of Si particles was significantly reduced and Si was distributed more homogeneously within Al-Si alloy.
- (2) The mechanical properties were improved significantly by adding Zr. The best results were for Zr content of 2.4 wt %. The tensile strength, compressive strength, shear strength, and hardness of Al-Si alloy with 2.4 wt % Zr reached 231.1 MPa, 343.1 MPa, 174.9 MPa, and 85.5 HV, respectively.
- (3) The fracture surface of Al-Si alloy without Zr additive showed a brittle fracture mode and no pits in the surface. When Zr was added, the Al-Si alloys exhibited a typical plastic deformation and a large amount of pits were formed.

Acknowledgments: This work is supported by “Chu-Ying” program of Southwest Jiaotong University, Thousand Talents Program of Sichuan province, and the Fundamental Research Funds for the Central Universities (2682016CX071).

Author Contributions: Hui Qian and Degui Zhu conceived and designed the experiments. Hui Qian performed the experiments. Hui Qian and Degui Zhu analyzed the data. Degui Zhu contributed reagents/materials/analysis tools. Hui Qian, Chunfeng Hu, and Xiaosong Jiang wrote the paper.

Conflicts of Interest: The authors declare no conflict of interest.

References

1. Miracle, D.B. Metal matrix composites—From science to technological significance. *Compos. Sci. Technol.* **2005**, *65*, 2526–2540. [[CrossRef](#)]
2. Hort, N.; Huang, Y.D.; Kainer, K.U. Intermetallics in Magnesium Alloys. *Adv. Eng. Mater.* **2006**, *8*, 235–240. [[CrossRef](#)]
3. Guo, Z.X.; Derby, B. Solid-state fabrication and interfaces of fibre reinforced metal matrix composites. *Prog. Mater. Sci.* **1995**, *39*, 411–495. [[CrossRef](#)]
4. Harrigan, W.C. Commercial processing of metal matrix composites. *Mater. Sci. Eng. A* **1998**, *244*, 75–79. [[CrossRef](#)]
5. Alizadeh, A.; Abdollahi, A.; Rafar, M.J. Processing, characterization, room temperature mechanical properties and fracture behavior of hot extruded multi-scale B₄C reinforced 5083 aluminum alloy based composites. *Trans. Nonferr. Met. Soc. China* **2017**, *27*, 1233–1247. [[CrossRef](#)]

6. ElSebaie, O.; Samuel, A.M.; Samuel, F.H.; Doty, H.W. The effects of mischmetal, cooling rate and heat treatment on the eutectic Si particle characteristics of A319.1, A356.2 and A413.1 Al–Si casting alloys. *Mater. Sci. Eng. A* **2008**, *480*, 342–355. [[CrossRef](#)]
7. Chomsaeng, N.; Haruta, M.; Chairuangri, T.; Kurata, H.; Isoda, S.; Shiojiri, M. HRTEM and ADF-STEM of precipitates at peak-ageing in cast A356 aluminum alloy. *J. Alloys Compd.* **2010**, *496*, 478–487. [[CrossRef](#)]
8. Tsai, Y.C.; Chou, C.Y.; Lee, S.L.; Lin, C.K.; Lin, J.C.; Lim, S.W. Effect of trace La addition on the microstructures and mechanical properties of A356 (Al–7Si–0.35Mg) aluminum alloys. *J. Alloys Compd.* **2009**, *487*, 157–162. [[CrossRef](#)]
9. Dobrzanski, L.A.; Weodarczyk, A.; Adamiak, M. The structure and properties of PM composite materials based on EN AW-2124 aluminum alloy reinforced with the BN or Al₂O₃ ceramic particles. *J. Mater. Process. Technol.* **2006**, *175*, 186–191. [[CrossRef](#)]
10. Turralba, J.M.; Dacost, C.E.; Velasco, F. P/M aluminum matrix composites: An overview. *J. Mater. Process. Technol.* **2003**, *133*, 203–206. [[CrossRef](#)]
11. Kang, H.S.; Yoon, W.Y.; Kim, K.H.; Kim, M.H.; Yoon, Y.P.; Cho, I.S. Effective parameter for the selection of modifying agent for Al–Si alloy. *Mater. Sci. Eng. A* **2007**, *449*, 334–337. [[CrossRef](#)]
12. AlMangour, B.; Grzesiak, D.; Jenn, M.Y. Selective laser melting of TiC reinforced 316L stainless steel matrix nanocomposites: Influence of starting TiC particle size and volume content. *Mater. Des.* **2016**, *104*, 141–151. [[CrossRef](#)]
13. AlMangour, B.; Grzesiak, D.; Jenn, M.Y. Rapid fabrication of bulk-form TiB₂/316L stainless steel nanocomposites with novel reinforcement architecture and improved performance by selective laser melting. *J. Alloys Compd.* **2016**, *680*, 480–493. [[CrossRef](#)]
14. Emadi, D.; Rao, A.K.P.; Mahfoud, M. Influence of scandium on the microstructure and mechanical properties of A319 alloy. *Mater. Sci. Eng. A* **2010**, *527*, 6123–6132. [[CrossRef](#)]
15. Prukkanon, W.; Srisukhumbowornchai, N.; Limmaneevichitr, C. Modification of hypoeutectic Al–Si alloys with scandium. *J. Alloys Compd.* **2009**, *477*, 454–460. [[CrossRef](#)]
16. Pandee, P.; Patakhar, U.; Limmaneevichitr, C. Microstructural evolution and mechanical properties of Al-7Si-0.3Mg alloys with erbium additions. *J. Alloys Compd.* **2017**, *728*, 844–853. [[CrossRef](#)]
17. Gao, Z.H.; Li, H.Y.; Lai, Y.Q. Effects of minor Zr and Er on microstructure and mechanical properties of pure aluminum. *Mater. Sci. Eng. A* **2013**, *580*, 92–98. [[CrossRef](#)]
18. Sepehrband, P.; Mahmudi, R.; Khomamizadeh, F. Effect of Zr addition on the aging behavior of A319 aluminum cast alloy. *Scr. Mater.* **2005**, *52*, 253–257. [[CrossRef](#)]
19. Liu, W.Y.; Xiao, W.L.; Xu, C. Synergistic effects of Gd and Zr on grain refinement and eutectic Si modification of Al–Si cast alloy. *Mater. Sci. Eng. A* **2017**, *693*, 93–100. [[CrossRef](#)]
20. Slipenyuk, A.; Kuprin, V.; Milman, Y.; Goncharuk, V.; Eckert, J. Properties of P/M processed particle reinforced metal matrix composites specified by reinforcement concentration and matrix-to-reinforcement particle size ratio. *Acta Mater.* **2006**, *54*, 157–166. [[CrossRef](#)]
21. Smagorinski, M.E.; Tsantrizos, P.G.; Grenier, S.; Cvasin, A.; Brzezinski, T.; Kim, G. The properties and microstructure of Al-based composites reinforced with ceramic particles. *Mater. Sci. Eng. A* **1998**, *244*, 86–90. [[CrossRef](#)]
22. Ryum, N. Precipitation and recrystallization in an Al-0.5 wt % Zr-alloy. Precipitation et recristallisation dans un alliage Al-0.5% Zr (en poids). Ausscheidung und rekristallisation in einer Al-0.5gew.% Zr-Legierung. *Acta Metall.* **1969**, *17*, 269–278. [[CrossRef](#)]
23. Robson, J.D.; Prangnell, P.B. Dispersoid precipitation and process modelling in zirconium containing commercial aluminum alloys. *Acta Metall.* **2001**, *49*, 599–613. [[CrossRef](#)]
24. Wang, F.; Qiu, D.; Liu, Z.L. The grain refinement mechanism of cast aluminum by zirconium. *Acta Mater.* **2013**, *61*, 5636–5645. [[CrossRef](#)]

